Electron paramagnetic resonance study of Gd^{3+} centres in cubic and hexagonal perovskite $RbZnF_3$ crystals

1997 J. Phys.: Condens. Matter 9 5193

(http://iopscience.iop.org/0953-8984/9/24/016)

J. Phys.: Condens. Matter **9** (1997) 5193–5204. Printed in the UK PII: S0953-8984(97)80645-5

Electron paramagnetic resonance study of Gd^{3+} centres in cubic and hexagonal perovskite $RbZnF_3$ crystals

M Arakawa†, H Ebisu† and H Takeuchi‡

† Department of Physics, Nagoya Institute of Technology, Nagoya 466, Japan
‡ Department of Information Electronics, School of Engineering, Nagoya University, Nagoya 464-01, Japan

Received 3 January 1997

Abstract. EPR measurements have been made on Gd^{3+} centres in single crystals of $RbZnF_3$ at room temperature using an X-band spectrometer. In crystals doped with Gd^{3+}, both spectra with cubic and spectra with tetragonal symmetries are observed. These centres are ascribed to Gd^{3+} ions substituted for Rb^+ ions in cubic $RbZnF_3$ (c-$RbZnF_3$) without any local charge compensation and with a vacancy at its nearest Rb^+ site, respectively. In some as-grown crystals co-doped with Gd^{3+} and Li^+, signals from a new trigonal centre are observed in place of those from the cubic and tetragonal centres in c-$RbZnF_3$. The trigonal centre is identified as the Gd^{3+}–Li^+ pair substituted for the Zn^{2+}–Zn^{2+} bond in a Zn_2F_9 unit in hexagonal $RbZnF_3$ (h-$RbZnF_3$), although the cubic perovskite structure is normally stabilized at room temperature. This indicates that the Gd^{3+}–Li^+ pairs in Zn_2F_9 units may be related to the crystal growth of the hexagonal structure in the matrix.

1. Introduction

It is known that there are many ABF_3-type compounds, where A and B respectively stand for monovalent alkali metal and divalent metal elements. These compounds were classified according to the tolerance factor for perovskite structure defined as

$$t = (r_A + r_F)/\sqrt{2}(r_B + r_F)$$

where r_A, r_B, and r_F are respectively the ionic radii of the A^+, B^{2+}, and F^- ions. That is, cubic perovskite-type structure with space group $Pm3m$ is classified by t in the range 0.88–1.00, and hexagonal $BaTiO_3$- (h-$BaTiO_3$-) type structure with space group $P6_3/mmc$ is classified by t in the range 1.00–1.06 [1, 2]. The crystal structure of $RbZnF_3$ ($t = 1.00$) is at the boundary between the cubic perovskite and h-$BaTiO_3$ type structures. $RbZnF_3$ crystallizes in the hexagonal phase (h-$RbZnF_3$) from a stoichiometric melt at 730 ± 10 °C. Upon cooling, it normally undergoes a destructive phase transition at about 640 °C and becomes cubic (c-$RbZnF_3$) [3]. Recently, single crystals of h-$RbZnF_3$ were obtained by the Czochralski technique at room temperature by quick extraction of the boule from the melt at an approximate rate of 200 K per second in order to inhibit the structural phase transition [3].

The h-$RbZnF_3$ crystals are interesting because of their close relation to both $KNiF_3$-like cubic perovskite and $CsNiCl_3$-like hexagonal crystals. This structure may be regarded as an intermediate between the $CsNiCl_3$ structure, which consists of infinite linear arrays of octahedra sharing faces, and the perovskite structure, which consists of a three-dimensional

0953-8984/97/245193+12$19.50

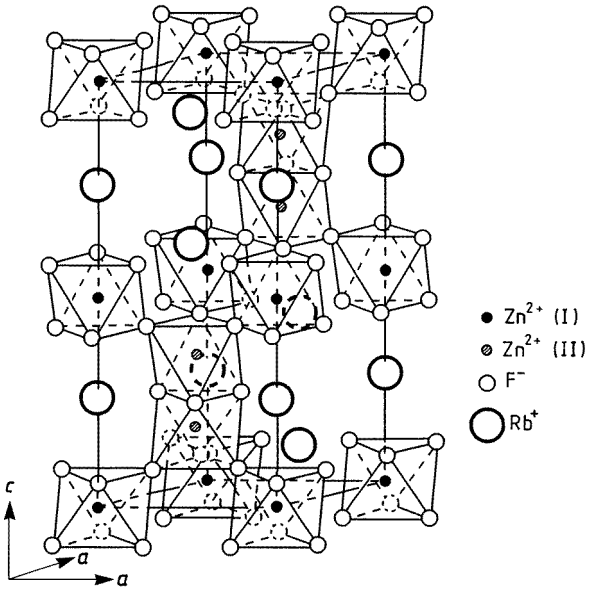

Figure 1. The unit cell of h-$RbZnF_3$.

network of octahedra sharing corners—that is, two octahedra sharing a face form a $[Zn_2F_9]^{5-}$ unit, which shares corners with six different ZnF_6 octahedra, as seen in figure 1. The Zn^{2+} ions in this lattice occupy two crystallographically inequivalent sites (I and II), where sites I are in ZnF_6 octahedra and sites II are in Zn_2F_9 units.

We have carried out EPR measurements on single crystals of $RbZnF_3$ doped with Gd^{3+} and co-doped with Gd^{3+} and Li^+. In as-grown crystals doped with Gd^{3+}, signals from cubic and tetragonal Gd^{3+} centres were observed. The results suggest that the crystal has cubic perovskite structure at room temperature. On the other hand, in some as-grown crystals co-doped with Gd^{3+} and Li^+, signals from a new trigonal centre were observed at room temperature in place of those from the cubic and tetragonal centres in c-$RbZnF_3$. This suggests that the hexagonal structure in the matrix is obtained at room temperature by co-doping with Gd^{3+} and Li^+ via a normal cooling procedure.

In this paper we will report the EPR results for the cubic and tetragonal Gd^{3+} centres formed in c-$RbZnF_3$, and the trigonal Gd^{3+}–Li^+ centre formed in h-$RbZnF_3$ single crystals.

2. Experimental procedures

Single crystals of $RbZnF_3$ doped with Gd^{3+} and co-doped with Gd^{3+} and Li^+ were grown in graphite crucibles by the Bridgman technique. Gd metal (99.9%) and LiF powder were used for doping the starting mixtures of ZnF_2 and RbF. The mixtures were heated to about 800 °C to yield liquid mixtures under an argon atmosphere. Then the temperature was lowered to 300 °C with a cooling rate of 50 °C h^{-1}. The single crystals of c-$RbZnF_3$ were obtained in the batch doped with Gd^{3+}. In the batch co-doped with Gd^{3+} and Li^+, some single crystals of h-$RbZnF_3$ were obtained. The h-$RbZnF_3$ crystals obtained have some natural planes with hexagonal symmetry about the *c*-axis. The measurements were made at room temperature using a JES-FE1XG ESR spectrometer operating in the X-band, at the Centre for Instrumental Analysis at Nagoya Institute of Technology. The numerical computations were performed by the computer at the Computation Centre at Nagoya University.

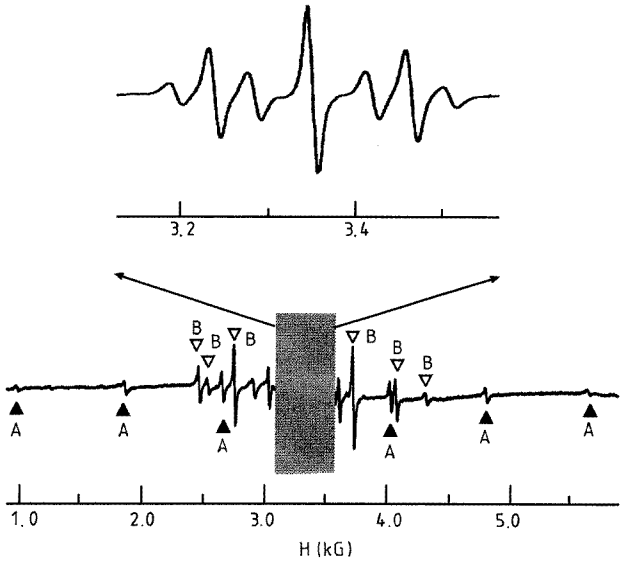

Figure 2. EPR spectra of the Gd^{3+} centres observed in c-$RbZnF_3$ with $\boldsymbol{H} \parallel [100]$ at room temperature. The intense spectrum is represented on a larger scale.

3. Results

The ground state of the Gd^{3+} ion which results from a $4f^7$ configuration is $^8S_{7/2}$. A recorder trace of the EPR signals observed in the [100] field direction at 300 K is shown in figure 2 for an as-grown crystal of c-$RbZnF_3$. The signals clearly indicate the presence of two distinct Gd^{3+} centres. One is an intense spectrum in the field range of about 3.2–3.6 kG, and the other is a much weaker one in the range of about 1.0–6.0 kG.

3.1. The EPR spectrum of Gd^{3+} with cubic symmetry in c-$RbZnF_3$

The intense spectrum in the [100] field direction is represented on a larger scale in figure 2. The seven fine-structure signals are well revealed. The total fine-structure spread shows a maximum in this direction. The angular variations of their resonance fields show dependences of 90° periodicity in the {001} planes. These results indicate the intense spectrum to be of cubic symmetry. In a cubic crystal field, the EPR spectrum is well described by the following spin Hamiltonian:

$$\mathcal{H} = g\beta \boldsymbol{S} \cdot \boldsymbol{H} + \frac{1}{60} b_4 (O_4^0 + 5O_4^4) + \frac{1}{1260} b_6 (O_6^0 - 21O_6^4) \tag{1}$$

where the principal x-, y-, and z-axes are chosen to be parallel to the crystalline [100], [010], and [001] axes. The zero-field splitting parameters b_4 and b_6 could be determined from the resonance fields of the seven well resolved signals when $\boldsymbol{H}$ is parallel to the [100] direction. The spin-Hamiltonian parameters obtained are listed in table 1, together with those for cubic centres in perovskite fluorides [4–6]. We select a negative sign for b_4, like those for the cubic centres in table 1.

3.2. EPR spectra of Gd^{3+} with tetragonal symmetry in c-$RbZnF_3$

The EPR spectrum observed in the [100] field direction in c-$RbZnF_3$ is equivalent to those in the [010] or [001] directions. The weak spectrum in the [100] field direction is composed

Table 1. Values of the spin-Hamiltonian parameters for the cubic Gd^{3+} centre in c-$RbZnF_3$ at room temperature, together with those for cubic centres in perovskite fluorides. The R are metal–ligand distances in the matrix crystals. The units are 10^{-4} cm^{-1} for b_4 and b_6.

Crystal	R (Å)	g	b_4	b_6	Coordination	Reference
$KMgF_3$	1.994	1.9916(5)	−11.15(5)	1.20(5)	12	[5]
$KZnF_3$	2.027	1.992(1)	−8.95(5)	1.13(5)	12	[4]
c-$RbZnF_3$	2.055	1.992(1)	−8.03(1)	1.07(2)	12	This work
$RbCdF_3$	2.200	1.992(1)	−4.44(5)	0.82(5)	6	[6]
$RbCaF_3$	2.227	1.992(1)	−4.92(5)	0.83(5)	6	[6]
$CsCdF_3$	2.230	1.992(1)	−4.82(5)	0.86(5)	6	[6]
$CsCaF_3$	2.262	1.992(1)	−5.49(5)	0.89(5)	6	[6]

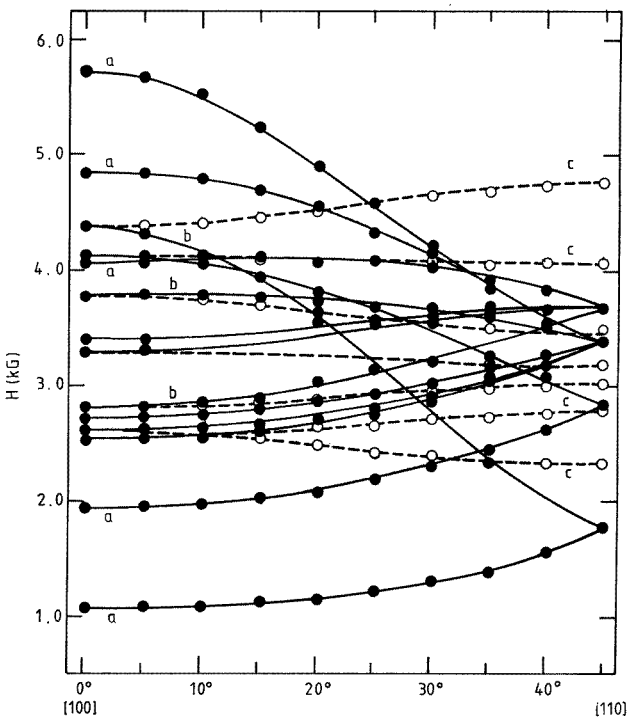

Figure 3. The angular variation of the signals A and B marked in figure 2 with $\boldsymbol{H}$ in the (001) plane. The smooth curves indicate the angular variation computed using the parameters for the best fit. The full and dotted lines marked a, b, and c denote a set of calculated branches, where the tetragonal axes are parallel to the [100], [010], and [001] directions, respectively.

of two types of signal, marked A and B in figure 2. The field direction dependences of the signals A and B in the (001) plane are shown in figure 3. Each signal A is composed of one branch labelled a having a peak or trough in the [100] field direction. When $\boldsymbol{H}$ is rotated a few degrees away from the [100] direction, each signal marked B splits further into two branches labelled b and c, as seen in figure 3. Branches c are almost constant, but show slight dependences of 90° periodicity. The other branches, b, which have peaks or troughs in the [100] direction, coincide with the branches a for the [110] direction. The signals A and B are exchanged for the [010] field direction. This makes it clear that the weak spectra

have tetragonal symmetry, and that the branches a, b, and c are due to Gd^{3+} ions associated with charge compensation along the [100], [010], and [001] crystalline axes, respectively.

Table 2. Values of the spin-Hamiltonian parameters for the tetragonal Gd^{3+} centre in c-$RbZnF_3$ at room temperature. The upper signs of b_n^m are appropriate, as mentioned in section 4.1. The units are 10^{-4} cm^{-1} for b_n^m.

Crystal	g	b_2^0	b_4^0	b_4^4	b_6^0	b_6^6
c-$RbZnF_3$	1.992(1)	$\mp$347.6(1)	$\mp$4.42(2)	$\mp$72.8(3)	$\pm$0.98(4)	$\mp$23.8(6)

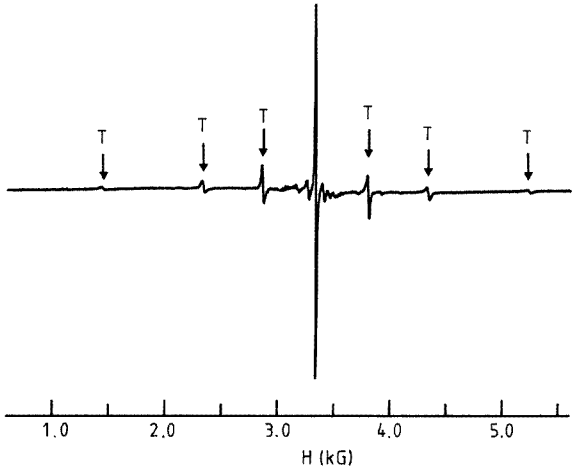

Figure 4. EPR spectra of the Gd^{3+} centres observed in h-$RbZnF_3$ with $\boldsymbol{H} \parallel \boldsymbol{c}$ at room temperature. The arrows labelled T denote the signals from the new trigonal centre.

The tetragonal spectra have been described by the following spin Hamiltonian:

$$\mathcal{H} = g\beta \boldsymbol{S} \cdot \boldsymbol{H} + \frac{1}{3} b_2^0 O_2^0 + \frac{1}{60}(b_4^0 O_4^0 + b_4^4 O_4^4) + \frac{1}{1260}(b_6^0 O_6^0 + b_6^4 O_6^4) \qquad (2)$$

where the z-axis is the direction having maximum total spread parallel to one of the crystalline axes. The x- and y-axes are chosen to be the directions parallel to the other crystalline axes. The spectra observed were fitted to the spin Hamiltonian by the matrix-diagonalization method using a computer. The relative signs of the b_n^m can be uniquely determined. The spin-Hamiltonian parameters obtained are listed in table 2. Full and dotted curves in figure 3 show the theoretical curves calculated using the spin-Hamiltonian parameters listed in table 2. Good agreement of the calculated values of the resonance field with the experimental ones is obtained.

3.3. The EPR spectrum of Gd^{3+} with trigonal symmetry in h-$RbZnF_3$

A new spectrum was observed in some crystals obtained from one batch co-doped with Gd^{3+} and Li^+. In this crystal, signals from the cubic and tetragonal centres observed in c-$RbZnF_3$ disappear. This result suggests that the h-$RbZnF_3$ structure may be formed by co-doping with Gd^{3+} and Li^+, although the cubic perovskite structure is normally stabilized at room temperature. The hexagonal structure of the matrix is confirmed by x-ray diffraction analysis. Typical EPR spectra for h-$RbZnF_3$ are shown in figure 4 for $\boldsymbol{H}$ parallel to the crystalline c-axis. The total spread of the seven fine-structure signals is a maximum in

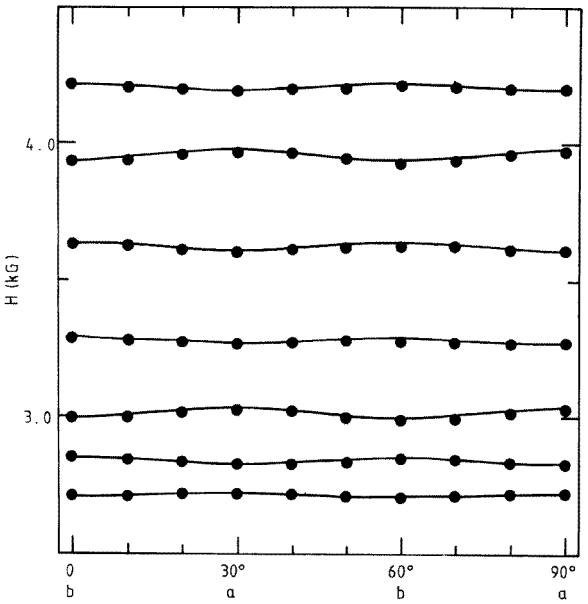

Figure 5. The angular variation of the EPR spectrum of the trigonal Gd^{3+} centre in h-$RbZnF_3$ with $\boldsymbol{H}$ in the c-plane. The labels a and b correspond respectively to the directions for the minimum and maximum fine-structure spreads in this figure. The smooth curves indicate the angular variation computed using the parameters for the best fit.

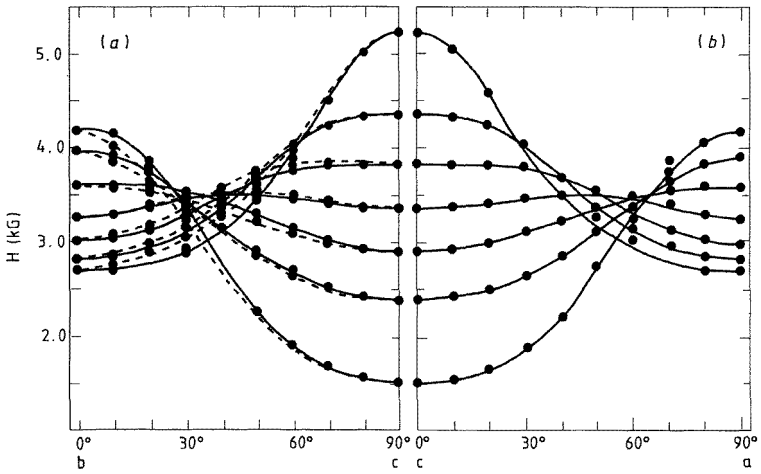

Figure 6. Angular variations of the EPR spectra for h-$RbZnF_3$ with $\boldsymbol{H}$ in (*a*) the plane perpendicular to the direction a, and (*b*) the plane perpendicular to the direction b defined in figure 5. The smooth curves indicate the angular variation computed using the parameters for the best fit. The full and dotted lines show the calculated branches for the centres, where the principal x-axes parallel to the direction b differ from each other by 180°.

this direction. The angular dependence of the signals in the c-plane is represented in figure 5. The seven fine-structure signals observed are almost constant, but some show

slight dependences of 60° periodicity. The field directions of the minimum and maximum fine-structure spreads in figure 5 are called the directions a and b hereafter. The angular dependences of the fine-structure signals when $\boldsymbol{H}$ is rotated in the planes perpendicular to the directions a and b are represented in figures 6(*a*) and 6(*b*), respectively. Each signal observed in the *c*-direction splits further into two branches, as seen in figure 6(*a*). In figure 6(*b*) the two branches coincide with each other. The results suggest the presence of two equivalent trigonal centres which rotate by 60° with respect to each other about the *c*-axis in h-$RbZnF_3$.

Table 3. Values of the spin-Hamiltonian parameters for the trigonal Gd^{3+} centre in h-$RbZnF_3$ at room temperature. The upper signs of b_n^m are appropriate, as mentioned in section 4.2. The units are 10^{-4} cm^{-1} for b_n^m.

Crystal	g	b_2^0	b_4^0	b_4^3	b_6^0	b_6^3	b_6^6
h-$RbZnF_3$	1.992(1)	∓256.3(3)	∓9.1(1)	±85(6)	∓1.7(2)	∓26(6)	∓17(2)

The trigonal spectra have been described by the following spin Hamiltonian:

$$\mathcal{H} = g\beta \boldsymbol{S}\cdot\boldsymbol{H} + \frac{1}{3}b_2^0 O_2^0 + \frac{1}{60}(b_4^0 O_4^0 + b_4^3 O_4^3) + \frac{1}{1260}(b_6^0 O_6^0 + b_6^3 O_6^3 + b_6^6 O_6^6) \qquad (3)$$

where the *z*-axis denotes the trigonal axis parallel to the *c*-axis. The *x*- and *y*-axes are chosen to be parallel to the directions b and a. The spectra observed were fitted to the spin Hamiltonian by the matrix-diagonalization method using a computer. The spin-Hamiltonian parameters obtained are listed in table 3. The relative signs of the b_n^m-parameters can be uniquely determined. Full and dotted curves in figure 6 show the theoretical curves calculated using the spin-Hamiltonian parameters listed in table 3. Good agreement of the calculated values of the resonance field with the experimental ones is obtained.

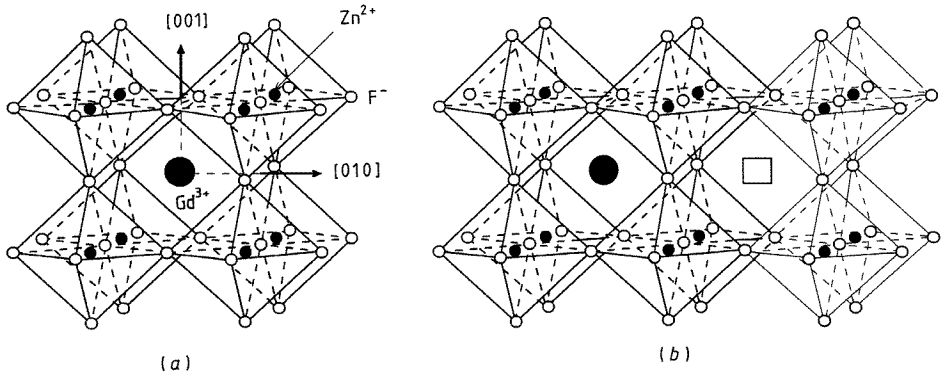

Figure 7. A schematic model for (*a*) the cubic centre, and (*b*) the tetragonal centre in c-$RbZnF_3$.

4. Discussion

4.1. Cubic and tetragonal Gd^{3+} centres in c-$RbZnF_3$

Cubic perovskite fluorides normally have monovalent and divalent cations surrounded by twelve and six nearest fluorine neighbours respectively. In Cd^{2+} or Ca^{2+} compounds, the

Gd^{3+} ion substitutes for a Cd^{2+} or Ca^{2+} site in sixfold coordination [6, 7]. In contrast with the Cd^{2+} or Ca^{2+} ions, Mg^{2+} and Zn^{2+} are not replaced by Gd^{3+} due to their small ionic radii. In cubic perovskite crystals such as $KZnF_3$ [4] and $KMgF_3$ [5], Gd^{3+} substitutes for a K^+ site in twelvefold coordination. The parameter of b_4 for a cubic centre in sixfold coordination has a magnitude and a lattice constant dependence that are empirically different from that for the centre in twelvefold coordination, as seen in table 1—that is, its magnitude for twelvefold coordination is about twice the size of that for sixfold coordination, and tends to become smaller with increasing lattice constant, contrary to that for sixfold coordination. For the cubic Gd^{3+} centre in c-$RbZnF_3$, the magnitude of b_4 and its tendency as regards the lattice constant dependence indicate the substitution of a Gd^{3+} ion for a Rb^+ site in twelvefold coordination, as seen in figure 7(*a*).

Table 4. Values of b_4 for cubic centres, and values of cubic parameters for the vacancy-associated tetragonal centres in perovskite fluorides. The units are 10^{-4} cm^{-1} for b_4, b_{2a}, b_{4a}, and b_{4c}.

Crystal	b_4	b_{2a}	b_{4a}	b_{4c}	b_{4c}/b_4	Reference
c-$RbZnF_3$	−8.03	−347.6	10.14	−14.56	1.81	This work
$RbCdF_3$	−4.44	−291.3	6.20	−8.32	1.85	[6, 8]
$RbCaF_3$	−4.92	−274.9	5.72	−8.58	1.74	[6, 8]
$CsCdF_3$	−4.82	−315.1	6.90	−9.28	1.93	[6, 8]
$CsCaF_3$	−5.49	−314.7	6.91	−9.96	1.81	[6, 8]

The tetragonal centre in c-$RbZnF_3$ is considered to be a Gd^{3+} ion associated with local charge compensation along the tetragonal axis parallel to a crystalline axis. The response of the cubic components of the crystal field to the fine structure begins from the fourth-rank term. We focus our attention on the second- and fourth-rank fine-structure terms for the tetragonal Gd^{3+} centre. Then we can represent the fine-structure terms by uniaxial and cubic terms in the same x-, y-, and z-coordinate system as follows:

$$\frac{1}{3}b_2^0O_2^0+\frac{1}{60}[b_4^0O_4^0+b_4^4O_4^4]=\frac{1}{3}b_{2a}O_2^0+\frac{1}{60}b_{4a}O_4^0+\frac{1}{60}b_{4c}[O_4^0+5O_4^4] \tag{4}$$

where the uniaxial and cubic parameters are expressed as

$$b_{2a}=b_2^0 \qquad b_{4a}=b_4^0-\frac{1}{5}b_4^4 \qquad b_{4c}=\frac{1}{5}b_4^4. \tag{5}$$

The cubic parameter b_{4c} can be expected to have a negative sign, similarly to b_4 for cubic centres in table 1. This suggests a negative sign for the parameter b_4^4, by equation (5). We therefore conclude that upper signs of b_n^m in table 2 are appropriate. The values of b_{4a} and b_{4c} for the tetragonal centre in c-$RbZnF_3$ are listed in table 4, together with the values of the second-rank uniaxial parameter b_{2a} ($=b_2^0$). The parameters for the tetragonal Gd^{3+} centres observed in ABF_3 cubic perovskite fluorides with vacancies at the nearest B^{2+} sites (the Gd^{3+}–V_B centres) [8] are also listed for comparison.

Two things are clear from this table. The first is that the values of b_{2a}, b_{4a}, and b_{4c} for the tetragonal centre in c-$RbZnF_3$ are of the same order, but their magnitudes are larger than those for the Gd^{3+}–V_B centres in cubic perovskite fluorides. Secondly, the ratio of b_{4c} to b_4 becomes almost the same value as those for the Gd^{3+}–V_B centres. This indicates that for the tetragonal centre a charge compensation may be associated with Gd^{3+} at its nearest cation site along a crystalline axis, and that the parameter b_{4c} correlates with the b_4 for the cubic centre in the same matrix, similarly to the case for Cd^{2+} and Ca^{2+} compounds. We

therefore conclude that the tetragonal centre in c-$RbZnF_3$ can be ascribed to a Gd^{3+} ion substituted for a Rb^+ site with a vacancy at its nearest Rb^+ site along a crystalline axis, as seen in figure 7(*b*). To the authors' knowledge, this centre constitutes the first EPR report of a Gd^{3+} ion in twelvefold coordination with charge compensation nearby.

It must be emphasized that for the Gd^{3+}–V_{Rb} pair the excess doubly positive charge on the Gd^{3+} is locally not just compensated by a Rb^+ vacancy. The formation of a Gd^{3+} centre with a vacancy at the nearest Zn^{2+} site is readily conceivable because of the excess positive charge on the Gd^{3+} being just compensated by a Zn^{2+} vacancy. Spectra of this Gd^{3+}–V_{Zn} pair are expected to be of trigonal symmetry along ⟨111⟩ directions, and so can be distinguished from those for the Gd^{3+}–V_{Rb} centres. But spectra with trigonal symmetry were not observed in c-$RbZnF_3$.

4.2. Trigonal Gd^{3+} centres in h-$RbZnF_3$

Spectra of the trigonal Gd^{3+} centres in h-$RbZnF_3$ were observed from as-grown crystals co-doped with Gd^{3+} and Li^+. The hexagonal structure may be regarded as an intermediate between the $CsNiCl_3$ structure, which consists of infinite linear arrays of octahedra sharing faces, and the perovskite structure, which consists of a three-dimensional network of octahedra sharing corners. From the EPR spectra, the presence of the two equivalent trigonal centres with trigonal axes parallel to the *c*-axis, which rotate by 60° with respect to each other about the *c*-axis, is confirmed. The trigonal centres are ascribed to a Gd^{3+} ion associated with a Li^+ ion along the *c*-axis.

First, we consider the possibility that Gd^{3+} substitutes for a Rb^+ site, like in c-$RbZnF_3$. Then, the formation of a Gd^{3+}–Li^+ pair is restricted to substitution for a Rb^+–Zn^{2+} pair in the matrix, because of the local charge compensation of excess positive charge on Gd^{3+} at a Rb^+ site. Several kinds of Rb^+–Zn^{2+} pair must be possible for this substitution, whose pair directions deviate from the *c*-axis, together with those along the *c*-axis. However, the directions of the pair axis observed are confirmed to be parallel to the *c*-axis. Substitution of the Gd^{3+}–Li^+ pair for a Rb^+–Zn^{2+} bond may be related to the formation of a Gd^{3+}–V_{Zn} pair, which is not recognized in c-$RbZnF_3$. We conclude that the Gd^{3+} ion for the trigonal centre in h-$RbZnF_3$ does not substitute for Rb^+, unlike the cubic and tetragonal centres in c-$RbZnF_3$.

Secondly, we consider the possibility that Gd^{3+} substitutes for a Zn^{2+} site. The Zn^{2+} ions in this lattice occupy two crystallographically inequivalent sites (I and II), where sites I are in ZnF_6 octahedra and sites II are in Zn_2F_9 units, as seen in figure 1. The surroundings of site I can be considered locally to be same as those for the cubic perovskite structure. The Gd^{3+} therefore does not substitute for a site I, like that in c-$RbZnF_3$. In a unit cell, there are two Zn_2F_9 units which rotate by 60° with respect to each other about the *c*-axis, as seen in figure 8. Signals from the two trigonal centres observed in figure 6(*a*) are consistent with the Gd^{3+}–Li^+ pairs in these two types of Zn_2F_9 unit. The two Zn_2F_9 units in figure 8 are equivalent with the directions in the plane from the *c*-axis to the crystalline *a*-axis. The fact that the two branches coincide with each other in figure 6(*b*) indicates the principal *y*-axis (the direction a) to be parallel to the crystalline *a*-axis. We conclude that the trigonal centre in h-$RbZnF_3$ is identified as a Gd^{3+}–Li^+ pair substituted for the Zn^{2+}–Zn^{2+} bond in a Zn_2F_9 unit.

The surroundings of site II can be considered as a part of a $CsNiCl_3$-like hexagonal structure with infinite linear arrays of octahedra sharing faces. In this type of hexagonal crystal—e.g. in $RbMgBr_3$ [9], $CsMgBr_3$ [10], and $CsMgCl_3$ [10]—Gd^{3+} ions substitute for Mg^{2+} sites in spite of the small ionic radii of the Mg^{2+} ions substituting for Gd^{3+} ions. In

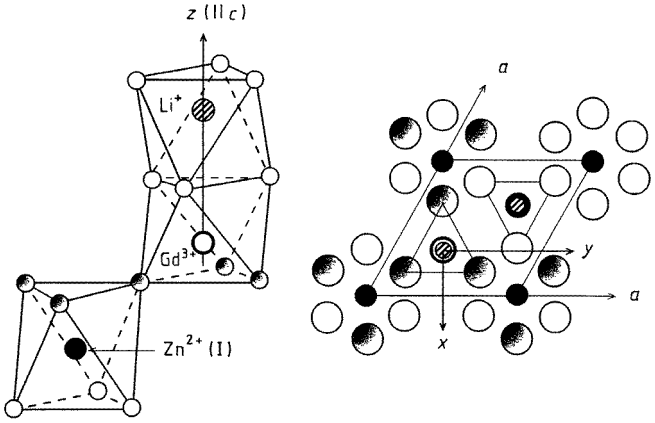

Figure 8. A schematic model for the trigonal centre in h-$RbZnF_3$, and a projection of an h-$RbZnF_3$ crystal onto the *c*-plane. Two Zn_2F_9 units in the unit cell are represented by triangles. The Gd^{3+}–Li^+ pairs in these units correspond to the two branches in figure 6(*a*). The *x*-, *y*-, and *z*-axes denote the coordination system in which the spin Hamiltonian is described. The principal *y*-axis direction (the direction a) is parallel to the crystalline *a*-axis.

these crystals, the excess positive charges of Gd^{3+} ions are compensated by the forming of a Gd^{3+}–Li^+ pair [9] replacing a Mg^{2+}–Mg^{2+} bond or a Gd^{3+}–V_{Mg}–Gd^{3+} pair [10] replacing a Mg^{2+}–Mg^{2+}–Mg^{2+} bond in the linear arrays of the octahedra. The similar formation of a Gd^{3+}–Li^+ pair might be possible in h-$RbZnF_3$ to substitute for the Zn^{2+}–Zn^{2+} bond in a Zn_2F_9 unit.

Table 5. Values of the uniaxial, cubic, and hexagonal parameters for the Gd^{3+} centres in h-$RbZnF_3$ at room temperature, together with those for trigonal centres in perovskite compounds and $RbMgBr_3$ at 465 K, in the high-temperature phase of the $CsNiCl_3$-type structure. The units are 10^{-4} cm^{-1}.

Crystal	Centre	b_{2a}	b_{4a}	b_{6a}	b_{4c}	b_{6c}	b_{6h}	Reference
h-$RbZnF_3$	Gd^{3+}–Li^+	−256.3	−12.1	−3.8	−4.5	1.2	−37	This work
$RbCaF_3$	Gd^{3+}–V_{Rb}	80.1	7.87	−0.36	−0.74	0.91	−2.5	[11]
$CsCaCl_3$	Gd^{3+}–V_{Cs}	3.3	1.2	0.46	−13	0.25	13	[12]
$RbMgBr_3$	Gd^{3+}–Li^+	391	23.5	—	−2.2	—	—	[9]

Like Takeuchi *et al* [10], for the case of the trigonal Gd^{3+} centre, we separate the fine-structure terms for the trigonal Gd^{3+}–Li^+ centre into uniaxial, cubic, and hexagonal terms up to the sixth-rank Stevens operators as follows:

$$\begin{aligned}\frac{1}{3}b_2^0O_2^0+\frac{1}{60}(b_4^0O_4^0+b_4^3O_4^3)+\frac{1}{1260}(b_6^0O_6^0+b_6^3O_6^3+b_6^6O_6^6)\\ =\frac{1}{3}b_{2a}O_2^0+\frac{1}{60}\left[b_{4a}O_4^0+b_{4c}\left(-\frac{2}{3}O_4^0-\frac{40\sqrt{2}}{3}O_4^3\right)\right]\\ +\frac{1}{1260}\left[b_{6a}O_6^0+b_{6c}\left(\frac{16}{9}O_6^0-\frac{140\sqrt{2}}{9}O_6^3+\frac{154}{9}O_6^6\right)+b_{6h}O_6^6\right].\end{aligned}\tag{6}$$

Equation (6) is valid when the following conditions are satisfied:

$$b_{2a} = b_2^0 \qquad b_{4a} = b_4^0 - \frac{1}{20\sqrt{2}}b_4^3 \qquad b_{6a} = b_6^0 + \frac{4}{35\sqrt{2}}b_6^3$$
$$b_{4c} = -\frac{3}{40\sqrt{2}}b_4^3 \qquad b_{6c} = -\frac{9}{140\sqrt{2}}b_6^3 \qquad b_{6h} = b_6^6 + \frac{11}{10\sqrt{2}}b_6^3. \tag{7}$$

The parameter b_4^3 for the trigonal centre is related to the cubic component of the fine-structure term by equation (7). This suggests a positive sign for b_4^3. We therefore conclude that the upper signs of b_n^m in table 3 are appropriate for the trigonal centre in h-$RbZnF_3$. The values of the axial parameters b_{na} ($n = 2, 4, 6$), the cubic parameters b_{nc} ($n = 4, 6$), and the hexagonal parameter b_{6h} calculated using equations (7) are listed in table 5. The parameters for the Gd^{3+}–V_{Rb} centre in $RbCaF_3$ [11] and the Gd^{3+}–V_{Cs} centre in $CsCaCl_3$ [12] are listed for comparison. In $RbMgBr_3$ with $CsNiCl_3$-type hexagonal structure [9], the parameters b_2^0, b_4^0, and b_4^3 for the Gd^{3+}–Li^+ centre were observed at 465 K, where the relative signs of the parameters were determined. The parameters b_{2a}, b_{4a}, and b_{4c} for this centre are calculated from these parameters by assuming a negative sign for b_{4c}. The results are also listed in this table. The axial parameters b_{2a} and b_{4a} for the trigonal Gd^{3+}–Li^+ centre in h-$RbZnF_3$ have different signs from those for other trigonal centres, as seen in table 5.

The positive sign of b_{2a} for the Gd^{3+}–V_{Rb} centre in $RbCaF_3$ results from an effective positive charge distribution along the trigonal axis caused by distortions of the ligand octahedron. This arises from the deviations of the ligand fluorines away from the trigonal axis caused by the presence of the Rb^+ vacancy, similarly to the case for the Fe^{3+}–V_K centre in $KZnF_3$ observed by ENDOR measurements [13]. As a result, the ligand octahedron is compressed along the trigonal axis. The positive sign of b_{2a} for the Gd^{3+}–Li^+ centre in $RbMgBr_3$ suggests that the Gd^{3+} ion with its large ionic radius tends to compress the ligand octahedron. The negative sign of b_{2a} for the Gd^{3+}–Li^+ centre in h-$RbZnF_3$ shows conversely elongation of the ligand octahedron.

In $CsNiCl_3$-type crystals, octahedra sharing faces make the neighbouring Ni^{2+}–Ni^{2+} distances shorter than those in cubic perovskite crystals. The Coulomb repulsion between the neighbouring divalent cations elongates the octahedra along the c-axis. In $CsMgCl_3$ with $CsNiCl_3$-type structure, the formations of the several kinds of Cr^{3+} centre are identified by EPR measurements [14, 15]. The distortion of the ligand octahedron is quite sensitive to the association of the charge compensation at the nearest Mg^{2+} site—that is, the values of b_{2a} ($=b_2^0$) are $+1253.3 \times 10^{-4}$ cm^{-1} for the Cr^{3+} centre without any local compensation (the uncompensated centre), $\pm 86.6 \times 10^{-4}$ cm^{-1} for the Cr^{3+} centre associated with the Li^+ ion (the Cr^{3+}–Li^+ centre), and -2811×10^{-4} cm^{-1} for the Cr^{3+} centre associated with the Mg^{2+} vacancy (the Cr^{3+}–V_{Mg} centre) [15]. The elongation of the ligand octahedron is confirmed by the positive sign of b_{2a} for the uncompensated centre. The parameters b_{2a} show that the elongation of the ligand octahedron almost disappears for the Cr^{3+}–Li^+ centre, and changes into a compression for the Cr^{3+}–V_{Mg} centre. This indicates that the local distortion of the ligand octahedron results from the Coulomb repulsion between the charges on the nearest Mg^{2+} sites. In h-$RbZnF_3$, the octahedra of the Zn_2F_9 unit can be considered to be strongly elongated by the substitution of Gd^{3+} for a Zn^{2+} site because of the excess positive charge on Gd^{3+}. The negative value of b_{2a} for the Gd^{3+}–Li^+ pair in a Zn_2F_9 unit shows that the elongation is still maintained by the presence of the Li^+ at the other Zn^{2+} site in the Zn_2F_9 unit. This elongation is reasonable because the Gd^{3+} ion with a Zn^{2+} vacancy in the Zn_2F_9 unit can be considered as an isolated Gd^{3+} ion in an almost undistorted ligand octahedron, because of the lack of repulsive force from the other Zn^{2+}

ion in the unit.

The Zn_2F_9 units in h-$RbZnF_3$ are essential if one is to construct a hexagonal structure similar to the ZnF_6 octahedra. The Gd^{3+}–Li^+ pair in a Zn_2F_9 unit might be expected to be stable, like uncompensated centres in octahedra, because of the excess charge on the Gd^{3+} ion being just compensated by Li^+. It must be emphasized that crystals of h-$RbZnF_3$ are obtained by co-doping with Gd^{3+} and Li^+. This indicates that the Gd^{3+}–Li^+ pairs in Zn_2F_9 units may be related to the crystal growth of the hexagonal structure in the matrix.

5. Conclusions

The formation of c-$RbZnF_3$ at room temperature is confirmed by EPR spectra from the cubic and tetragonal Gd^{3+} centres observed in $RbZnF_3$ doped with Gd^{3+}. The cubic centre has been identified as the substitutional Gd^{3+} centre at a Rb^+ site in twelvefold coordination. The tetragonal centre has been identified as the substitutional Gd^{3+} centre at a Rb^+ site with a nearest Rb^+ vacancy, although the excess doubly positive charge on the Gd^{3+} is locally not just compensated by the Rb^+ vacancy. This centre constitutes the first report of a Gd^{3+} ion in twelvefold coordination with charge compensation nearby. In some as-grown crystals co-doped with Gd^{3+} and Li^+, signals from a new trigonal centre were observed in the place of those from the cubic and tetragonal centres in c-$RbZnF_3$. The trigonal centre is identified as the Gd^{3+}–Li^+ pair substituted for the Zn^{2+}–Zn^{2+} bond in a Zn_2F_9 unit in h-$RbZnF_3$. The formation of the hexagonal structure at room temperature is confirmed by x-ray diffraction analysis. The h-$RbZnF_3$ crystals are formed by co-doping with Gd^{3+} and Li^+, although the cubic perovskite structure is normally stabilized at room temperature. This indicates that the Gd^{3+}–Li^+ pairs in Zn_2F_9 units may be related to the crystal growth of the hexagonal structure in the matrix.

Acknowledgments

The authors are grateful to Dr Masahiro Mori for useful measurements of x-ray diffraction. This work has been supported by a Grant-in-Aid for Scientific Research on Priority Areas: ‘New Development of Rare Earth Complexes’, No 08220231, from The Ministry of Education, Science and Culture of Japan.

References

[1] Babel D 1967 *Struct. Bonding* **3** 1–87
[2] Babel D 1969 *Z. Anorg. Chem.* **369** 117–30
[3] Daniel Ph, Toulouse J, Gesland J Y and Rousseau M 1995 *Phys. Rev.* B **52** 9129–32
[4] Arakawa M, Ebisu H, Yosida T and Horai K 1979 *J. Phys. Soc. Japan* **46** 1483–7
[5] Abraham M M, Finch C B, Kolopus J L and Lewis J L 1971 *Phys. Rev.* B **3** 2855–64
[6] Arakawa M, Aoki H, Takeuchi H, Yosida T and Horai K 1982 *J. Phys. Soc. Japan* **51** 2459–63
[7] Buzaré J Y, Fayet-Bonnel M and Fayet J C 1981 *J. Phys. C: Solid State Phys.* **14** 67–81
[8] Arakawa M, Ebisu H and Takeuchi H 1985 *J. Phys. Soc. Japan* **54** 3577–83
[9] Kirklin K H and McPherson G L 1983 *J. Phys. C: Solid State Phys.* **16** 6539–50
[10] Henling L M and McPherson G L 1977 *Phys. Rev.* B **16** 4756–60
[11] Takeuchi H, Arakawa M and Ebisu H 1995 *J. Phys.: Condens. Matter* **7** 1417–26
[12] Vaills Y and Buzaré J Y 1987 *J. Phys. Chem. Solids* **48** 363–70
[13] Krebs J J and Jeck R K 1972 *Phys. Rev.* B **5** 3499–505
[14] McPherson G L and Devancy K O 1980 *J. Phys. C: Solid State Phys.* **13** 1735–43
[15] Takeuchi H, Tanaka H and Arakawa M 1993 *J. Phys.: Condens. Matter* **5** 9205–14